INTERNATIONAL JOURNAL FOR NUMERICAL METHODS IN FLUIDS, VOL. 16, 461–487 (1993)

TRANSIENT SIMULATION OF 2D AND 3D STRATIFIED AND INTERMITTENT TWO-PHASE FLOWS. PART I: THEORY

RANDI MOE

Institutt for energiteknikk, PO Box 40, 2007 Kjeller, Norway

AND

KJELL H. BENDIKSEN

Institute of Mathematics, Department of Mechanics, University of Oslo, PO Box 1053, Blindern, Norway

SUMMARY

Stratified and intermittent stratified-bubble (slug) flows are complex phenomena, often requiring transient 2D and 3D descriptions. This paper presents the physical basis of a new type of multidimensional two-fluid model, particularly suited for transient flow problems. Important constitutive relations for wall shear stress and interfacial momentum transfer with necessary assumptions and simplifications are discussed. The numerical method is based on an implicit finite difference scheme, solved directly in two steps applying a separate equation for the pressure. The model has been verified through extensive comparisons with available experimental data as well as through comparisons with other models.

KEY WORDS Transient 2D and 3D simulation Two-phase flow Stratified and intermittent flows

1. INTRODUCTION

Over the last few years, transportation of multiphase flow has become increasingly important to economic and efficient offshore production of oil and gas. It is now possible to develop small and marginal fields by transporting unprocessed well flow to nearby installations, utilizing the existing infrastructure. Main well flow components are oil, gas and water. The high investment costs of offshore production facilities for oil and gas significantly narrow the margins of error with respect to design and safe and reliable operation of such systems. Consequently, since the 1970s the petroleum industry has directed considerable R&D efforts towards improving two-phase 1D design tools. In particular, the need for better experimental verification of closure laws was recognized, and large scale high pressure pipeline test facilities were erected, e.g. the Sintef Multiphase Flow Laboratory at Tiller, Norway.[1,15,31] One-dimensional simulation tools are now available to calculate the pressure drop, liquid contents, flow regimes and temperature profiles, e.g. OLGA,[1] PLAC[2] and PEPITE.[3] Transient situations such as terrain slugging may also be investigated using OLGA or PLAC. These models are based on a semi-mechanistic approach, critically dependent on empirical correlations describing friction between the phases, wall friction and flow regimes.

Finer details of multiphase flow presently have to be studied through extensive experiments, as only in special cases can the multidimensional models be applied with confidence. For two-phase

0271–2091/93/060461–27$18.50

Received May 1992
Revised November 1992

flow, however, at least three general-purpose codes (FLUENT, FLOW-3D and PHOENICS) are available, and lots of other, more problem-oriented models, mainly based on the work of Patankar and Spalding.[4] These, however, are generally limited to dispersed flows or particle tracking.

For separated or stratified flow, Nichols *et al.*[5] proposed an algorithm to track a free surface or an interface between two fluids. This model did not take into account turbulence. Shoham and Taitel[6] and Issa[7] studied turbulent stratified flow over the cross-section of a pipe, and Akai *et al.*[8] and Line *et al.*,[9] among others, investigated planar flow in channels.

In general, the two-fluid equations in two or three dimensions are solved by iterative procedures. Several solution algorithms for two-phase flow exist IMF,[10] IPSA,[11] TOFFEA,[12] SIMPLE-2P[13] and PISO-2P.[14] These are all based on a sequence of three distinct steps where

1. the momentum equations for both phases are solved;
2. a new pressure field is determined; and
3. the volume fractions of each of the two phases are obtained.

These methods differ mainly in the ordering of the above sequence, particularly the stage at which the volume fraction is determined, as well as the degree of implicit–explicitness to which the equations are formulated.

In the proposed model the general two-fluid equations have been applied, with the assumption of a single pressure field. The modelling of constitutive laws at the interface is not general, but focused on separate or stratified flows. A basic difference between this model and the other existing models is in the solution procedure, aiming, in particular, at, improved predictions of transient problems.

The numerical scheme is based on an extension of the one-dimensional (1D) models of Bendiksen *et al.*[1,15] A 'volume' equation is applied for the pressure, enabling a direct two-step solution procedure. First, the pressure and velocities are solved implicitly from the volume and momentum equations and then the specific masses are solved from the continuity equations. These linearized equation sets are solved directly, applying a Gaussian band solver, avoiding an iterative solution procedure.

2. PHYSICAL TWO-FLUID MODEL

In the local instantaneous formulations of multiphase flow the domain is described by single-phase subsets separated by interfaces. The conservation equations for single-phase flow are applied within each subset, and local instantaneous transfer rates of mass, momentum and energy are formulated as boundary conditions at the interfaces.

Local time-averaged formulations may be expressed in two basically different descriptions:

1. Homogeneous flow models[16–18] (diffusion or drift flux models).
2. Two-fluid models.[18–21]

In the averaging process, important characteristics of the flow fields are lost and must be reintroduced into the model through appropriate closure laws.

2.1. Basic equations

In an Eulerian approach the time averaged two-fluid model equations for the liquid and gas phases ($k = l, g$) are usually expressed, see e.g. Vernier and Delhaye[19] and Ishii[18] assuming a single

(fluctating) time or spatial scale, as:

conservation of mass

$$\frac{\partial}{\partial t}(\alpha_k \rho_k) + \nabla \cdot (\alpha_k \rho_k \mathbf{u}_k) = \Gamma_k, \tag{1}$$

conservation of momentum

$$\frac{\partial}{\partial t}(\alpha_k \rho_k \mathbf{u}_k) + \nabla \cdot (\alpha_k \rho_k \mathbf{u}_k \mathbf{u}_k) = -\nabla(\alpha_k \rho_k) + \alpha_k \rho_k \mathbf{g} + \nabla \cdot [\alpha_k (\tau_k + \tau_k^{\mathrm{T}})] + \mathbf{M}_k, \tag{2}$$

conservation of energy

$$\frac{\partial}{\partial t}\left[\alpha_k \rho_k \left(e_k + \frac{\mathbf{u}_k^2}{2}\right)\right] + \nabla \cdot \left[\alpha_k \rho_k \left(e_k + \frac{\mathbf{u}_k^2}{2}\right)\mathbf{u}_k\right] = \nabla \cdot [\alpha_k (\mathbf{q}_k + \mathbf{q}_k^{\mathrm{T}})] + \nabla \cdot (\alpha_k \wp_k \cdot \mathbf{u}_k) + \alpha_k \rho_k \mathbf{g} \cdot \mathbf{u}_k + E_K, \tag{3}$$

and the continuity relation

$$\alpha_{\mathrm{g}} + \alpha_\ell + \alpha_{\mathrm{s}} = 1, \tag{4}$$

where all field variables are understood to be time-averaged quantities. Important exceptions requiring several time scales, include stratified wavy flows and heat transfer in dispersed bubbly flows. $\mathbf{u}_k$ denotes the velocity, p_k the pressure, ρ_k the density, e_k the internal energy, τ_k the viscous shear tensor, τ_k^{T} the turbulent flux, $\mathbf{q}_k$ the heat flux, $\mathbf{q}_k^{\mathrm{T}}$ the turbulent heat flux, $\wp_k$ the stress tensor, $\mathbf{g}$ the acceleration due to gravity and α_k the volume fraction of phase k. The terms Γ_k, $\mathbf{M}_k$ and E_K represent interfacial mass transfers due to phase change, interfacial momentum transfer and total energy transfer through interfaces, respectively.

Jump conditions. Standard time-averaged jump conditions for mass and momentum are applied, based on those of Ishii.[18] Conservation of mass across an interface is expressed as

$$\Gamma_{\mathrm{g}} + \Gamma_\ell = \Gamma_{\mathrm{s}}. \tag{5}$$

Assuming ideal massless interfaces of infinitesimal thickness, $\Gamma_{\mathrm{s}} = 0$, as well as $\alpha_{\mathrm{s}} = 0$ in (4). Similarly, the momentum balance at the interface must satisfy

$$\mathbf{M}_{\mathrm{g}} + \mathbf{M}_\ell = \mathbf{M}_{\mathrm{m}}, \tag{6}$$

where the momentum transfer at the interface for each phase, $\mathbf{M}_k$, to a first approximation may be expressed as

$$\mathbf{M}_k = \mathbf{M}_k^{\Gamma} + \mathbf{M}_k^{\mathrm{d}} + p_{k\mathrm{i}} \nabla \alpha_k - \tau_{k\mathrm{i}} \nabla \alpha_k - \tau_{k\mathrm{i}}^{\mathrm{T}} \nabla \alpha_k. \tag{7}$$

The first term on the right-hand side represents the momentum transfer due to mass transfer, and the second term represents the skin drag force and a possible normal component of the momentum transfer due to pressure discontinuity between the bulk phase and the interface ($p_{k\mathrm{i}} - p_k \neq 0$). The variables $\tau_{k\mathrm{i}}$ and $\tau_{k\mathrm{i}}^{\mathrm{T}}$ denote the viscous and turbulent shear stresses at the interface.

A possible interfacial momentum source may arise due to surface tension effects:

$$\mathbf{M}_{\mathrm{m}} = 2 \frac{\sigma}{R_{\ell \mathrm{g}}} \nabla \alpha_\ell + \mathbf{M}_{\mathrm{m}}^R. \tag{8}$$

The last term incorporates the effect of a possible change in the mean curvature. Effects due to changes in the surface tension gradient are neglected.

Finally, the energy balance at the interface may be expressed as

$$E_g + E_\ell = E_m. \tag{9}$$

The total energy transfer condition on the macroscopic scale, imposing similar approximations as for momentum transfer, can be expressed as follows:

$$E_k = E_{ki}^{\Gamma} - p_{ki}\frac{\partial \alpha_k}{\partial t} + \mathbf{M}_k^d \cdot \mathbf{u}_{ki} + W_{ki}^T + \frac{q_k''}{L_s}. \tag{10}$$

The first term on the right-hand side represents energy transfer due to mass transfer, W_{ki}^T is the work due to fluctuations in drag forces and q_k'' is the average heat transfer per interfacial area (energy gain), where $1/L_s$ is the total area concentration.

The mixture energy source is represented, imposing similar assumptions as for the mixture momentum source as

$$E_m = 2\frac{\sigma}{R_{\ell g}}\frac{\partial \alpha_\ell}{\partial t} + E_m^R. \tag{11}$$

2.2. *Closure relations and simplifications*

As a first approximation, focusing on detailed modelling of the flow structure rather than mass transfer, the energy equation has been omitted and a constant temperature field applied throughout. The present version also neglects mass transfer between the phases ($\Gamma_k = 0$). This is consistent with the assumption of a constant temperature field in time. The actual pressure differences are small for the type of stratified problems to be investigated, and the composition of the fluid is assumed to be constant.

The original model considers four pressures, one for each phase (p_k), and the pressures on each side of the interface (p_{ki}).

Under the above assumptions, neglecting surface tension, as shown by Ishii,[18] there is no pressure discontinuity across the interfaces, and a common pressure field may be applied: $p = p_\ell = p_g = p_i$.

Flow regime description. Multiphase flow, in general, is a very complicated phenomenon. It is conveniently classified into flow regimes which may be further grouped into two main types:

1. Dispersed flow (particles, bubbles or droplets).
2. Separated flow (stratified, annular or elongated bubbles).

More complex flow regimes often occur as combinations of these, such as stratified and annular flows with entrainment, and slug flow.

Dispersed flow regimes have been quite extensively studied recently using two- and three-dimensional models by several workers, including Johansen[22] and Ellull.[23]

The problem of closure in turbulent stratified flow has been investigated, among others, by Shoham and Taitel,[6] Issa,[7] Akai *et al.*[8] and Line *et al.*[9] The first two of these modelled the cross-section of a stratified pipe flow using a bipolar co-ordinate frame. This system enables the computational mesh to be fitted to the wall of the pipe and to the rectilinear interface simultaneously (tracking the interface). A single-phase turbulence model can be used within each phase. At the interface, boundary conditions can be applied directly. On the other hand, the works of Akai *et al.*[8] and Line *et al.*[9] are confined to planar flow, where also the interfacial conditions can be applied directly to the interface.

The present work is focused on problems related to separated flows, either stratified or elongated bubble flow.

Interfacial shear stress modelling. In time averaging the equations, information about the microscopic structure of the flow is lost. Relevant examples are fluctuations at the interfaces and detailed two-phase flow patterns.

Imposing the above assumptions, the jump conditions for the momentum balance reduce to the skin drag force, only:

$$\begin{aligned} \mathbf{M}_m &= 0, \\ \mathbf{M}_g &= -\mathbf{M}_\ell = \mathbf{M}_k^d. \end{aligned} \tag{12}$$

Two basically different approaches to interfacial momentum transfer are possible. Firstly, a no-slip condition may be imposed at the interface. This normally implies the use of boundary layer velocity functions and asymptotic matching, and becomes extremely difficult in the presence of waves.

In an alternative simpler approach applied for wavy surfaces, interfacial friction is modelled through an extension of the method applied in one-dimensional models.[15] Slip between the phases is allowed, and correct velocity profiles far from the interface must be obtained by proper choice of coefficients.

Assuming the drag force to be proportional to the velocity difference squared between the phases, this force can be expressed in Cartesian co-ordinates as

$$\begin{aligned} \mathbf{M}_\ell^x &= F_i^x |u_r| u_r; \qquad F_i^x = \frac{1}{2} \rho_g \lambda_i^x \frac{S_i}{A}, \\ \mathbf{M}_\ell^y &= F_i^y |v_r| v_r; \qquad F_i^y = \frac{1}{2} \rho_g \lambda_i^y \frac{S_i}{A}, \end{aligned} \tag{13}$$

where

$$\begin{aligned} u_r &= u_\ell - u_g, \\ v_r &= v_\ell - v_g. \end{aligned} \tag{14}$$

The interfacial perimeter, S_i, denotes the area of the interface and A is the volume of the actual flowfield. Although a simplification, the drag force (13) is quite general, and incorporates a variety of different physical interfacial conditions. Three different approaches regarding the interfacial friction factor have been investigated:

1. No interaction between the phases:

$$\lambda_i^x, \lambda_i^y \approx 0. \tag{15}$$

   This gives an inviscid (free-slip) boundary condition at the interface for elongated bubble flows at low (atmospheric) pressure. It, however, leads to a numerically unstable solution.

2. A very strong coupling in the main (axial) flow direction and no interaction in the transverse direction:

$$\begin{aligned} \lambda_i^y &= 10^{-3}, \\ \lambda_i^x &= 1{\cdot}0 \times 10^6. \end{aligned} \tag{16}$$

   This is, in principle, an unphysical boundary condition at the interface, but will nevertheless be shown to be practically applicable for many flow types, and to have clear numerical advantages.

3. Several other types of interfacial friction factors (λ_i) have been investigated. A modification of the Wallis[30] formula,

$$\lambda_i^x = \lambda_i^y = 0{\cdot}02(1+75h_\ell), \tag{17}$$

has been found to describe stratified or annular flows quite well.

Shear stress modelling. On the basis of the assumption of Newtonian fluids, the average stress tensor for laminar flow is normally expressed as for single-phase flow:

$$\tau_k = \mu_k(\nabla \mathbf{u}_k + \nabla \mathbf{u}_k^*) - [(\tfrac{2}{3}\mu_k - \lambda_k)\nabla \cdot \mathbf{u}_f \Im], \tag{18}$$

where μ_k and λ_k are the viscosity and the bulk viscosity of phase k. $\Im$ is the unit tensor, and all quantities are time-averaged.

In turbulent flow, neglecting possible effects due to interface fluctuations, the Reynolds stresses may be expressed as

$$\tau_k^T = -\overline{\rho_k \mathbf{u}_k' \mathbf{u}_k'}, \tag{19}$$

where $\mathbf{u}_k'$ represents the local velocity fluctuations of phase k.

For single-phase flow, the Boussinesq approach is applied to model turbulence. Average turbulent shear stresses are estimated as the product of the mean velocity gradient and a 'turbulent viscosity', μ_T which is dependent on the flow field,

$$-\overline{\rho_k \mathbf{u}_k' \mathbf{u}_k'} = \rho_k \mu_k^T [\nabla \mathbf{u}_k + \nabla \mathbf{u}_k^* - \tfrac{2}{3}(\nabla \cdot \mathbf{u}_k \Im)]. \tag{20}$$

For multiphase or two-phase flow this method cannot be adopted without further justification, as the macroscopic averaged equations contain interfaces which are no longer described separately, but through the volume fractions (α_k). The problem of turbulence in dispersed flow has been considered by several authors. Normally, it is accounted for in the continuous phase through a modified mixing length, a k–ε or a full Reynold stress model. The thesis by Ellull[23] provides a recent overview of the problem.

In our proposed model the Boussinesq approach to turbulence has been applied for each phase k:

$$\mu_{k,\,\mathrm{eff}} = \mu_k + \mu_k^T. \tag{21}$$

The turbulent eddy viscosity (μ_k^T) will display spatial variations for each phase and will also be influenced by the interface. For the flow probems studied in this work, the average flow parameters are not expected to be particularly sensitive to turbulent effects. Thus, the simple Prandtl mixing-length hypothesis has been applied as a first approach:

$$\mu^T = \rho l_m^2 \left| \frac{\partial u}{\partial y} \right|. \tag{22}$$

The formula of Nikuradse for single-phase flow, as described by Launder and Spalding[26] is used for the mixing length:

$$\frac{l_m}{H/2} = 0{\cdot}14 - 0{\cdot}08\left(1 - \frac{y}{H/2}\right)^2 - 0{\cdot}06\left(1 - \frac{y}{H/2}\right)^4, \tag{23}$$

where H denotes channel height or pipe diameter.

Equations (22) and (23) have been used in the proposed model with a straightforward extension of the turbulent viscosity:

$$\mu_k^T = \rho l_m^2 \left| \frac{\partial v_k}{\partial x} + \frac{\partial}{\partial y}(u_k \alpha_k) \right|. \tag{24}$$

Equation of state. The density of each phase is a function of pressure and temperature:

$$\rho_k = \rho_k(p, T). \tag{25}$$

A simple relation including compressibility is applied in the model:

$$\rho_k = \rho_{k,0} + \frac{\partial \rho_k}{\partial \mathrm{p}}(p - p_0) + \frac{\partial \rho_k}{\partial T}(T - T_0). \tag{26}$$

2.3. Proposed two-fluid model

Applying the above simplifications gives the following set of basic equations for each phase k:

conservation of mass

$$\frac{\partial}{\partial t}(\alpha_k \rho_k) + \nabla \cdot (\alpha_k \rho_k \mathbf{u}_k) = 0, \tag{27}$$

conservation of momentum

$$\frac{\partial}{\partial t}(\alpha_k \rho_k \mathbf{u}_k) + \nabla \cdot (\alpha_k \rho_k \mathbf{u}_k \mathbf{u}_k) = -\alpha_k \nabla p + \alpha_k \rho_k \mathbf{g} + \nabla \cdot [\alpha_k \mu_{k,\mathrm{eff}} (\nabla \mathbf{u}_k + \nabla \mathbf{u}_k^* - \tfrac{2}{3} \nabla \cdot \mathbf{u}_k \Im)] + \mathbf{F}_{ki} |\mathbf{u}_r| \mathbf{u}_r, \tag{28}$$

and the volume continuity relation

$$\alpha_\mathrm{g} + \alpha_\ell = 1. \tag{29}$$

The pressure equation. The tight coupling between pressure and velocities, in general, requires a simultaneous or iterative solution of the mass and momentum conservation equations. This, however, leads to rigid and time-consuming numerical procedures. An efficient and numerically robust solution of phase velocities and pressure is obtained by combining the two mass equations into a 'volume' equation, as proposed by Bendiksen *et al.*[1] for 1D models:

$$\left(\frac{\alpha_\mathrm{g}}{\rho_\mathrm{g}} \frac{\partial \rho_\mathrm{g}}{\partial p} + \frac{\alpha_\ell}{\rho_\ell} \frac{\partial \rho_\ell}{\partial p} \right) \frac{\partial p}{\partial t} = -\frac{1}{\rho_\mathrm{g}} \nabla \cdot (\alpha_\mathrm{g} \rho_\mathrm{g} \mathbf{u}_\mathrm{g}) - \frac{1}{\rho_\ell} \nabla \cdot (\alpha_\ell \rho_\ell \mathbf{u}_\ell). \tag{30}$$

2.4. Boundary and initial conditions

As stated, the proposed model is primarily intended for separated channel or pipe flow problems. The relevant boundary conditions along a wall will either be no-slip or free-slip (no friction at the wall).

At the inlet of a pipe or channel the velocities and volume fractions of each phase are specified. At the outlet a reference pressure and the volume fractions of the phases are specified. Applying these, a hydrostatic pressure profile over the pipe/channel height is calculated, and used as outlet-pressure-type boundary condition.

In the case of a closed box or pipe, the inlet velocities are set to zero, and a zero-velocity-type boundary condition is also imposed at the outlet.

As this is a transient model, start conditions must always be specified. Required conditions include volume fractions of the two phases over the entire flow domain and velocity fields set equal to the inlet conditions. The pressure field is calculated according to hydrostatic conditions.

Further details are presented in Section 3.3.

3. NUMERICAL METHOD

3.1. Solution procedure

The numerical solution procedure is based on a first-order semi-implicit finite difference scheme. A staggered mesh or Arakawa C-grid has been applied. This type of grid consists of cells where the velocities are defined on the boundaries and the pressures and specific masses are defined inside the volumes; see Figure 1. Expressing equations (1)–(4) in a conservative form, this scheme is volume- and mass-conserving if the equations were solved fully implicit. The solution of specific masses is decoupled from that of pressure and velocities. Thus, both mass and volume conservation may not be ensured. As described later, however, a correction has been implemented, giving both a mass- and volume-conserving scheme.

For clarity, we limit ourselves to the two-dimensional case. A three-dimensional model based on the same numerical methods is, however, operational and is now being tested out. In what follows, the indices j denote the x-direction, i the y-direction and n the time. Each discrete step is defined as follows:

$$\Delta x_j = x_{j+1} - x_j, \qquad j = 1, J, \tag{31}$$

$$\Delta y_i = y_{i+1} - y_i, \qquad i = 1, I, \tag{32}$$

$$\Delta t^{n+1} = t^{n+1} - t^n, \qquad n = 0, T. \tag{33}$$

The set of equations (60)–(62) is expressed in a mass-conserving form. An implicit solution of all variables in time implies an iterative method, or a stepwise solution of masses and velocities, separately. The equations have to be 'linearized' with respect to the product terms, e.g. fluxes, where 'old' masses from the previous time are used.

The applied semi-implicit method results in a split solution procedure at each time step. The required flow parameters and coefficients are updated based on the state vector (velocities, etc.) from the last time step. Velocities and pressures are then calculated from the momentum equations and the 'volume' equation, using specific masses and volume fractions from the previous time step. Finally, specific masses and volume fractions are calculated, based on updated densities and derivatives.

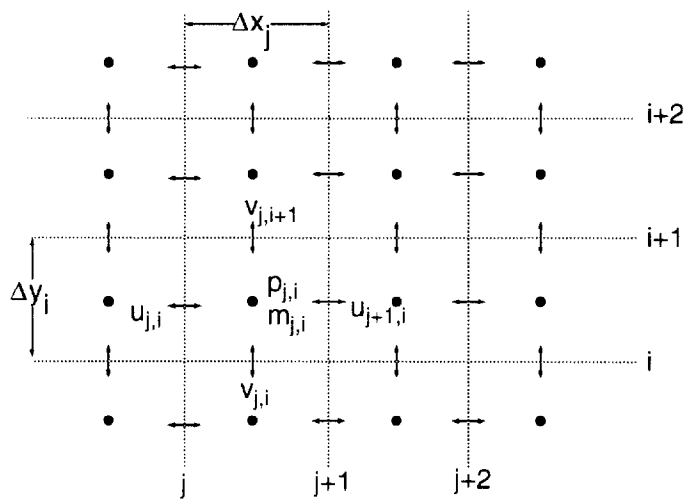

Figure 1. Finite difference staggered mesh scheme

Under the assumption of no interphasial mass transfer, the mass equations are decoupled, and may be solved separately. When specific masses and densities are known, the volume fractions can be obtained directly from the definition ($m_k \equiv \alpha_k \rho_k$). This set of equations is, however, over-determined, as the volume relation ($\alpha_g + \alpha_\ell = 1$) also applies. The solution method may, thus, give rise to an error in the specific volume, and an iterative volumetric correction procedure has to be included at each time step.

3.2. *Finite difference equations*

Time derivatives are generally defined as

$$(\delta_t F^{n+1})_{j,i} = \frac{1}{\Delta t}(F^{n+1}_{j,i} - F^{n}_{j,i}) \tag{34}$$

and spatial derivatives in the x- and y-dimension are defined as

$$\begin{aligned}(\delta_x F^n)_{j,i} &= \frac{1}{\Delta x_j}(F^n_{j+1,i} - F^n_{j,i}),\\ (\delta_y F^n)_{j,i} &= \frac{1}{\Delta y_i}(F^n_{j,i+1} - F^n_{j,i}),\end{aligned} \tag{35}$$

where $F^n_{j,i}$ denotes any variable. Definitions (34)–(35) apply to each phase k as well. For product terms, the derivatives with respect to time and the x-co-ordinate become

$$(\delta_t \overline{m^n_k u^{n+1}_k})_{j,i} = \frac{1}{\Delta t}[(\overline{m^n_k u^{n+1}_k})_{j,i} - (\overline{m^n_k u^n_k})_{j,i}], \tag{36}$$

$$[\delta_x (m^n_k u^{n+1}_k)^{\mathrm{up}}]_{j,i} = \frac{1}{\Delta x}[(m^n_k u^{n+1}_k)^{\mathrm{up}}_{j+1,i} - (m^n_k u^{n+1}_k)^{\mathrm{up}}_{j,i}], \tag{37}$$

where mean and upstream mass fluxes are applied in temporal and spatial terms, respectively, according to the following definitions:

$$(\bar{m}u)_{j,i} = \frac{m_{j-1,i}\Delta x_{j-1} + m_{j,i}\Delta x_j}{\Delta x_{j-1} + \Delta x_j} u_{j,i}. \tag{38}$$

$$(mu)^{\mathrm{up}}_{j,i} = \begin{cases} m_{j-1,i}u_{j,i} & \text{if} \quad u_{j,i} \geqslant 0, \\ m_{j,i}u_{j,i} & \text{if} \quad u_{j,i} < 0. \end{cases} \tag{39}$$

Discretization of the convective terms in the momentum equation may be performed in a number of ways. A reasonably stable suggestion is:

$$(\delta_x \overline{m^n_k u^n_k u^{n+1}_k}) = \begin{cases} \dfrac{1}{\Delta x_j}[(\overline{m^n_k u^n_k u^{n+1}_k})_{j,i} - (\overline{m^n_k u^n_k u^{n+1}_k})_{j-1,i}] & \text{if} \quad u^n_k \geqslant 0, \\ \dfrac{1}{\Delta x_j}[(\overline{m^n_k u^n_k u^{n+1}_k})_{j,i} - (\overline{m^n_k u^n_k u^{n+1}_k})_{j+1,i}] & \text{if} \quad u^n_k < 0, \end{cases} \tag{40}$$

and

$$[\delta_y \overline{(m_k v_k)^n u^{n+1}_k}] = \begin{cases} \dfrac{1}{\Delta y_i}\{[\overline{(m_k v_k)^n u^{n+1}_k}]_{j,i+1} - [\overline{(m_k v_k)^n u^{n+1}_k}]_{j,i}\} & \text{if} \quad \overline{(m_k v_k)^n} \geqslant 0, \\ \dfrac{1}{\Delta y_i}\{[\overline{(m_k v_k)^n u^{n+1}_k}]_{j,i} - [\overline{(m_k v_k)^n u^{n+1}_k}]_{j,i-1}\} & \text{if} \quad \overline{(m_k v_k)^n} < 0, \end{cases} \tag{41}$$

where it was found critical to apply the mean values of upstream mass flux, defined as follows:

$$\overline{(m_k v_k)}^n_{j,i} = \tfrac{1}{4}\left[(m_k v_k)^{\mathrm{up}}_{j,i} + (m_k v_k)^{\mathrm{up}}_{j,i+1} + (m_k v_k)^{\mathrm{up}}_{j-1,i} + (m_k v_k)^{\mathrm{up}}_{j-1,i+1}\right]^n. \tag{42}$$

The basic conservation equations (60)–(63) are discretized according to the above definitions and principles. In particular, the acceleration terms in the momentum equations are sensitive with respect to numerical stability. Mean masses are always applied, except for the cross terms (**uv**), where average upstream values, as defined by relation (41), are used. In the pressure terms, the minimum gas fraction and the maximum liquid fraction are used in the gas and liquid momentum equations, respectively. This gives correct results also for cases with sharp interfaces between the two phases, as well as improved numerical stability.

The proposed numerical model then reduces to:

conservation of mass

gas phase

$$[\delta_t m_g^{n+1} + \delta_x (m_g^{n+1} u_g^{n+1})^{\mathrm{up}} + \delta_y (m_g^{n+1} v_g^{n+1})^{\mathrm{up}}]_{j,i} = 0, \tag{43}$$

liquid phase

$$[\delta_t m_\ell^{n+1} + \delta_x (m_\ell^{n+1} u_\ell^{n+1})^{\mathrm{up}} + \delta_y (m_\ell^{n+1} v_l^{n+1})^{\mathrm{up}}]_{j,i} = 0, \tag{44}$$

the pressure equation

$$C_{j,i}\delta_t p^{n+1}_{j,i} + \frac{1}{\rho^n_{g,j,i}}[\delta_x (m_g^n u_g^{n+1})^{\mathrm{up}}]_{j,i} + \frac{1}{\rho^n_{g,j,i}}[\delta_x (m_g^n v_g^{n+1})^{\mathrm{up}}]_{j,i} + \frac{1}{\rho^n_{\ell,j,i}}[\delta_x (m_\ell^n u_\ell^{n+1})^{\mathrm{up}}]_{j,i} + \frac{1}{\rho^n_{\ell,j,i}}[\delta_x (m_\ell^n v_\ell^{n+1})^{\mathrm{up}}]_{j,i} = 0, \tag{45}$$

where

$$C_{j,i} = \frac{\alpha^n_{g,j,i}}{\rho^n_{g,j,i}}\left(\frac{\partial \rho_g}{\partial p}\right)^n_{j,i} + \frac{\alpha^n_{\ell,j,i}}{\rho^n_{\ell,j,i}}\left(\frac{\partial \rho_\ell}{\partial p}\right)^n_{j,i}. \tag{46}$$

conservation of momentum in x-direction (gas and liquid phase)

$$\begin{aligned}[\delta_t m_g^n u_g^{n+1} + \delta_x(\overline{m_g^n} u_g^n u_g^{n+1}) + \delta_y(\overline{(m_g v_g)^n} u_g^{n+1})]_{j,i} \\ = \min(\alpha^n_{g,j,i}, \alpha^n_{g,j-1,i})(\delta_x p^{n+1})_{j,i} - (m_g^n g \sin\varphi)_{j,i} \\ + [\delta_x(\alpha_g^n \mu^n_{g,\mathrm{eff}} \delta_x u_g^{n+1})_{j-i,i}] + [\delta_y(\overline{\alpha_g^n \mu^n_{g,\mathrm{eff}}} \delta_y u_g^{n+1})_{j,i-1}] + F^{x,n}_{j,i}(u_g^{n+1} - u_\ell^{n+1})_{j,i},\end{aligned} \tag{47}$$

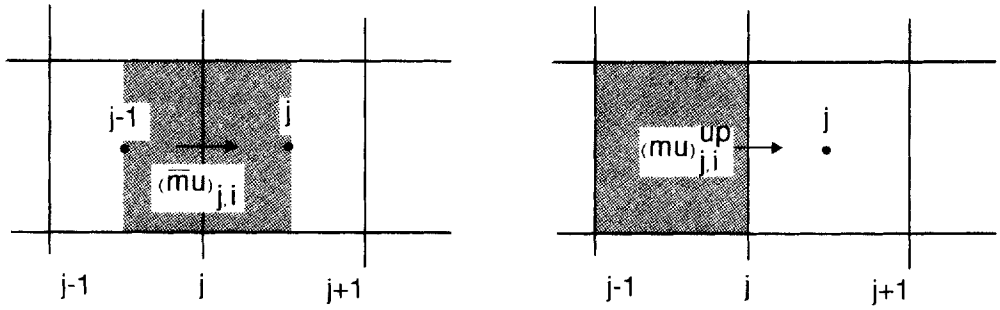

Figure 2. Two different discretizations of flux terms. (left: mean mass flux; right: upstream mass flux)

and

$$\{\delta_t m_\ell^n u_\ell^{n+1} + \delta_x(\overline{m_\ell^n u_\ell^n} u_\ell^{n+1}) + \delta_y[\overline{(m_\ell v_\ell)^n} u_\ell^{n+1}]\}_{j,i}$$
$$= \max(\alpha_{\ell,j,i}^n, \alpha_{\ell,j-1,i}^n)\{\delta_x p^{n+1}\}_{j,i} - \{m_\ell^n g \sin\varphi\}_{j,i} + \{\delta_x(\alpha_\ell^n \mu_{\ell,\text{eff}}^n \delta_x u_g^{n+1})_{j-i,i}\}$$
$$+ \{\delta_y(\overline{\alpha_\ell^n \mu_{\ell,\text{eff}}^n} \delta_y u_\ell^{n+1})_{j,i-1}\} + F_{j,i}^{x,n}(u_\ell^{n+1} - u_g^{n+1})_{j,i}. \tag{48}$$

conservation of momentum in y-direction (gas and liquid phase)

$$\{\delta_t m_g^n v_g^{n+1} + \delta_x((\overline{m_g^n u_g^n}) v_g^{n+1}) + \delta_y(\overline{m_g^n} v_g^n v_g^{n+1})\}_{j,i}$$
$$= \min(\alpha_{g,j,i}^n, \alpha_{g,j,i-1}^n)\{\delta_x p^{n+1}\}_{j,i} - \{m_g^n g \cos\varphi\}_{j,i} + \{\delta_x(\alpha_g^n \mu_{g,\text{eff}}^n \delta_x v_g^{n+1})_{j-1,i}\}$$
$$+ \{\delta_y(\overline{\alpha_g^n \mu_{g,\text{eff}}^n} \delta_y v_g^{n+1})_{j,i-1}\} + F_{j,i}^{x,n}(v_g^{n+1} - v_\ell^{n+1})_{j,i}, \tag{49}$$

and

$$\{\delta_t m_\ell^n u_\ell^{n+1} + \delta_x((\overline{m_\ell u_\ell}^n) v_\ell^{n+1}) + \delta_y(\overline{m_\ell^n} v_\ell^n v_\ell^{n+1})\}_{j,i}$$
$$= \max(\alpha_{\ell,j,i}^n, \alpha_{\ell,j,i-1}^n)\{\delta_x p^{n+1}\}_{j,i} - \{m_\ell^n g \cos\varphi\}_{j,i} + \{\delta_x(\alpha_\ell^n \mu_{\ell,\text{eff}}^n \delta_x v_g^{n+1})_{j-1,i}\}$$
$$+ \{\delta_y(\overline{\alpha_\ell^n \mu_\ell^n} \delta_y v_\ell^{n+1})_{j,i-1}\} + F_{j,i}^{x,n}(v_\ell^{n+1} - v_g^{n+1})_{j,i}. \tag{50}$$

As shown in Appendix II, the volumetric error puts additional restrictions on numerical accuracy and stability. The first term limits the local pressure changes in a given time step, depending upon the compressibility and density of the fluids. Limiting the volumetric error to 10^{-5} and assuming water as the dominating fluid, the model accepts local pressure transients of 0·1 bar per time step.

3.3. Boundary conditions

By applying a staggered mesh, the boundary conditions have to be imposed according to the location of the nodes. The boundary conditions along the walls can either be of a no-slip or a free-slip (no friction at the wall) type. Implementation of the boundary condition at the wall in the numerical scheme depends on the direction. For no-slip and free-slip conditions, antisymmetric and symmetric conditions are imposed for the tangential velocities, respectively. The normal velocities at the wall are set to zero, as indicated in Figure 3.

The boundary conditions at the walls are then expressed as follows:

No-slip	Free-slip
$u(x, \Delta y/2) = -u(x, -\Delta y/2),$	$u(x, \Delta y/2) = u(x, -\Delta y/2),$
$u(x, H-\Delta y/2) = -u(x, H+\Delta y/2),$	$u(x, H-\Delta y/2) = u(x, H+\Delta y/2),$
$v(x, 0) = 0,$	$v(x, 0) = 0,$
$v(x, H) = 0.$	$v(x, H) = 0.$

(51)

3.4. Solution matrices

In the proposed implicit solution procedure the equation systems form three matrix equations. The volume and momentum equations with a total of nine equations for each node constitute

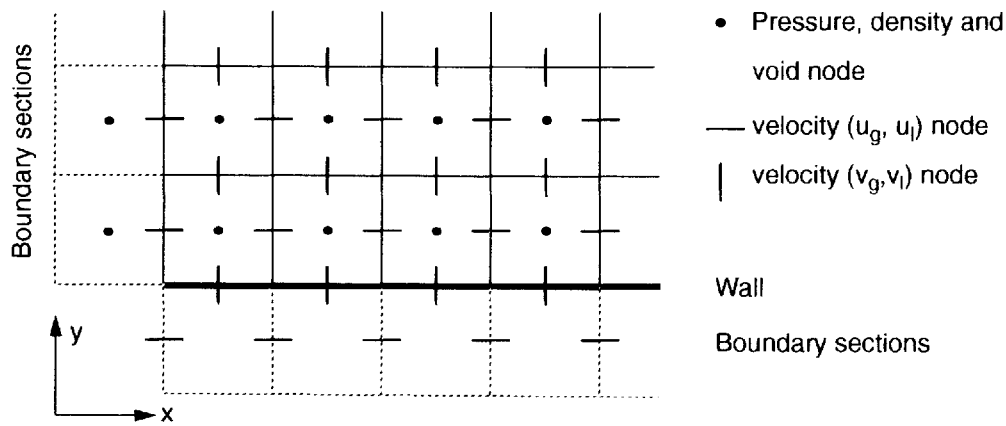

Figure 3. The numerical grid near the wall

a large matrix, and each of the two mass equations define separate matrices. As each variable couples only to adjacent nodes, a sparse band matrix structure results.

The momentum and volume matrix equation. The five equations for each grid boundary are ordered by starting with the momentum equations for gas and liquid in the x-direction, then the pressure equation and the momentum equations for gas and liquid in the y-direction, as indicated in Figure 4.

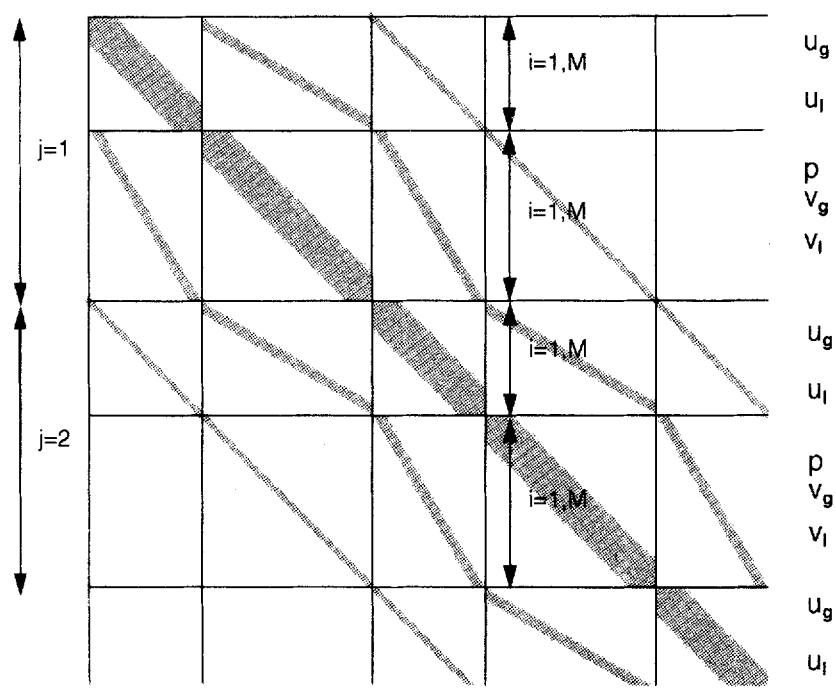

Figure 4. Matrix structure

The velocity in the main flow (x-) direction couples to the upstream and downstream velocities for the same phase, to the upstream and downstream pressures and the velocities of the same phase in the y-direction and to the velocity of the other phase. This gives a theoretical maximum of eight couplings. The same applies to the velocities in the transverse direction. The pressure of each node connects to the adjacent velocities and pressures, giving a total of nine couplings.

The equations form a sparse band matrix. For a system containing N nodes along the pipe or channel and M nodes in the transverse direction, the matrix will have a bandwidth of $10M-3$, and a length of $N(5M-2)$.

The applied Gaussian band algorithm is a very time- and space-consuming equation solver. The band consists of nine non-zero elements, and to simulate a typical channel, 7–10 nodes have been used across the height, giving a bandwidth between 67 and 97 elements.

Conjugate-gradient-like equation solvers have also been tested by Nossen[29] using incomplete LU-factorization (ILU) preconditioning. However, problems with convergence of these methods were encountered. This was mainly due to small main diagonal entries in the matrix caused by the pressure term in the volume equation. These terms are small, in particular, due to the low compressibility of the liquid phase.

The present 2D version of the model, using a total of 100 nodes in the x-direction and 25 nodes in the y-direction requires 25·1 MB of memory. The CPU time for each time step for a case sized 40×22 nodes is 80·5 s on a Hewlett Packard 9000/720 computer.

4. APPLICATIONS

The model is designed to cover a wide range of separated flows with volumetric gas fractions from 0 to 1. Single-phase flow is a special case, where the gas fraction or the liquid hold-up is zero. There are no restrictions on the range of fluid properties (density, viscosity or compressibility) that can be applied: the model in principle accepts any fluid, gas or liquid.

4.1. Single-phase flow

Laminar flow. The simplest test case consists of a horizontal channel applying the free-slip boundary condition at the walls. The calculation is initiated with a specified constant velocity profile at the inlet and proceeds for a few time steps. The model then gives a steady-state solution identical to the initial conditions to at least 5–6 digits.

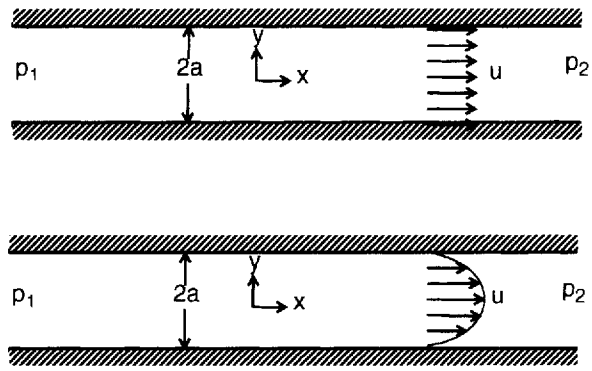

Figure 5. Channel flow (upper: free slip at the walls; lower: no slip at the walls)

Applying the no-slip boundary conditions at the walls yields the Poiseuille flow. Considering first the case of single-phase laminar channel flow ($\alpha_k = 1$), omitting the subscript k, equation (61) reduces to

$$-\frac{\partial p}{\partial x}+\frac{\partial}{\partial y}\left(\mu\frac{\partial u}{\partial y}\right)=0. \tag{52}$$

Applying the no-slip boundary condition at the channel walls

$$u=0, \qquad y=\pm a, \tag{53}$$

the familiar analytical solution is obtained as

$$u_a=\frac{3u_0}{2a^2}(a^2-y^2). \tag{54}$$

This solution cannot be directly compared with the numerical solution as the numerical scheme uses a different set of boundary conditions, where the velocity node lies half a mesh from the wall. By applying the 'numerical' boundary conditions

$$u(\pm a-\Delta y/2)=u(\pm a+\Delta y/2), \tag{55}$$

equation (52) gives

$$u_{an}=\frac{3u_0}{2a^2+\frac{3}{2}(\Delta y/2)^2}[a^2+(\Delta y/2)^2-y^2], \tag{56}$$

where u_0 is the mean velocity. The two analytical solutions (54), (56) are compared with the results from the numerical model (u_{nm}) in Table I.

Theoretically, a first-order finite difference scheme shall give exact results for an elliptic equation in Cartesian co-ordinates. Our results in Table I show that applying the proper 'numerical' boundary conditions, the numerical model confirms this to within the first five digits.

Similarly, for axisymmetric pipe flow, the equation for the Poiseuille flow becomes

$$-\frac{\partial p}{\partial x}+\frac{1}{r}\frac{\partial}{\partial r}\left(\mu\frac{\partial u}{\partial r}\right)=0. \tag{57}$$

The solution of equation (57) with no-slip boundary condition at the wall is given as

$$u_a=2u_0[1-(r/a)^2]. \tag{58}$$

Table I. Numerical and analytical velocity profiles for laminar Poiseuille flow in a channel

y (m)	u_a (m s^{-1})	u_{an} (m s^{-1})	u_{nm} (ms^{-1})
0·025	0·45830	0·48	0·480001
0·075	1·12500	1·12	1·119998
0·125	1·45833	1·44	1·439995
0·175	1·45833	1·44	1·439995
0·225	1·12500	1·12	1·119998
0·275	0·45830	0·48	0·480001

Imposing the 'numerical' boundary condition, the solution becomes

$$u_{an} = \frac{2u_0}{a^2 + 2\Delta r^2}(a^2 + \Delta r^2 - r^2). \tag{59}$$

The results of the two analytical solutions are compared with the results from the numerical model (u_{nm}) in Tables II and III, using five and nine nodes, respectively.

A first-order Euler finite difference scheme shall give a second-order error dependency on mesh size for axisymmetric co-ordinates.

The numerical results, u_{nm}, for both five and nine mesh points compare very well with the analytical solutions (with numerical boundary conditions) u_{an}. The relative error dependency on mesh size can be calculated for the radial position 0·225 m (for the examples in Tables II and III), and is shown in Figure 6.

Turbulent flow. For turbulent flow, the velocity profile will be modified. Figure 7(left) shows a turbulent velocity profile in channel flow and Figure 7(right) shows a turbulent velocity profile in axisymmetric pipe flow ($Re = 70\,000$ and $Re = 35\,000$, respectively).

The predicted turbulent velocity profiles give $u_{max} = 1{\cdot}28\,u_{mean}$ (for channel flow), which is slightly too high, and $u_{max} = 1{\cdot}45 u_{mean}$ for axisymmetric pipe flow, which is also too high. No effort was made to tune the simple turbulence model applied to get better results for the axisymmetric case, as improved models will be incorporated later.

Table II. Numerical and analytical velocity profiles for Poiseuille flow in a pipe of radius 0·45 m (five mesh points)

Radius (m)	u_a (m s^{-1})	u_{an} (m s^{-1})	u_{nm} (m s^{-1})
0·045	1·9800	1·9608	1·9650
0·135	1·8200	1·8039	1·8078
0·225	1·5000	1·4902	1·4934
0·315	1·0200	1·0196	1·0218
0·405	0·3800	0·3922	0·3930

Table III. Numerical and analytical velocity profiles for Poiseuille flow in a pipe of radius 0·45 m (nine mesh points)

Radius (m)	u_a (m s^{-1})	u_{an} (m s^{-1})	u_{nm} (m s^{-1})
0·025	1·9938	1·9877	1·9916
0·075	1·9444	1·9387	1·9424
0·125	1·8475	1·8405	1·8441
0·175	1·6975	1·6933	1·6965
0·225	1·5000	1·4969	1·4998
0·275	1·2531	1·2515	1·2540
0·325	0·9568	0·9571	0·9589
0·375	0·6111	0·6135	0·6147
0·425	0·2160	0·2209	0·2212

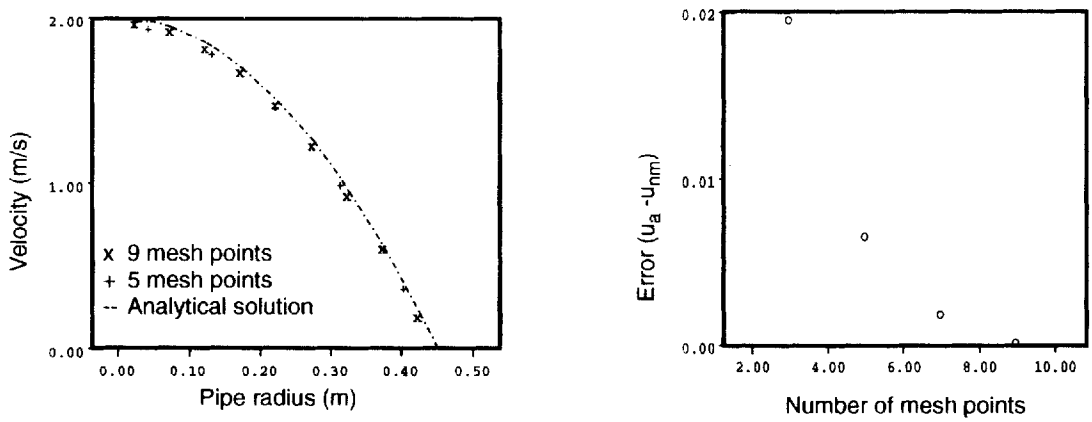

Figure 6. Axis symetric Poiseuille flow in a pipe with a mean velocity of 1·0 m s^{-1} (top: velocity profile; bottom: relative error)

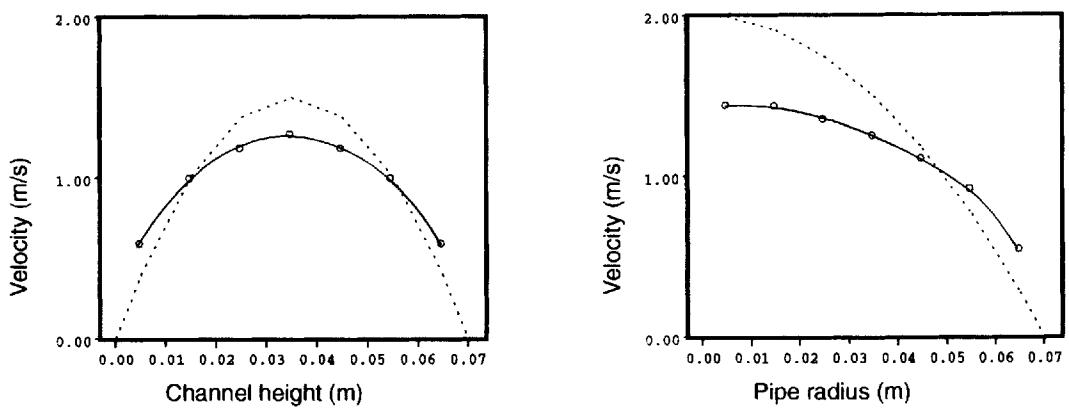

Figure 7. Turbulent pipe flow velocity profiles applying seven radial mesh points and a mean velocity of 1·0 m s^{-1} (–·–○–·–· turbulent flow, —— laminar flow) (left: channel flow; right: axisymmetric pipe flow)

4.2. Two-phase flow case studies

Consistence tests. Two sets of test cases have been run to check the symmetry properties of the model. First, a square box with sides of 2·2 m, initially filled with 50% of air and water evenly distributed within the total volume, was modelled, using 22 mesh points in both directions. Free-slip boundary conditions were applied at the walls. As shown in Figure 8, the two phases have been effectively separated after 0·8 s real time.

The second test case was similar to the first one, but tilted 45°. Here each box side was 0·7 m, and only seven mesh points were used in each direction. A no-slip boundary condition was applied at the walls.

Broken dam problem. A rectangular column of water in hydrostatic equilibrium is confined between two vertical walls and a horizontal bottom. The right wall is suddenly removed, and the water column starts to collapse under the influence of gravity. The initial water column is 1·0 m wide and 2·0 m high. Figure 10 shows the flow configuration.

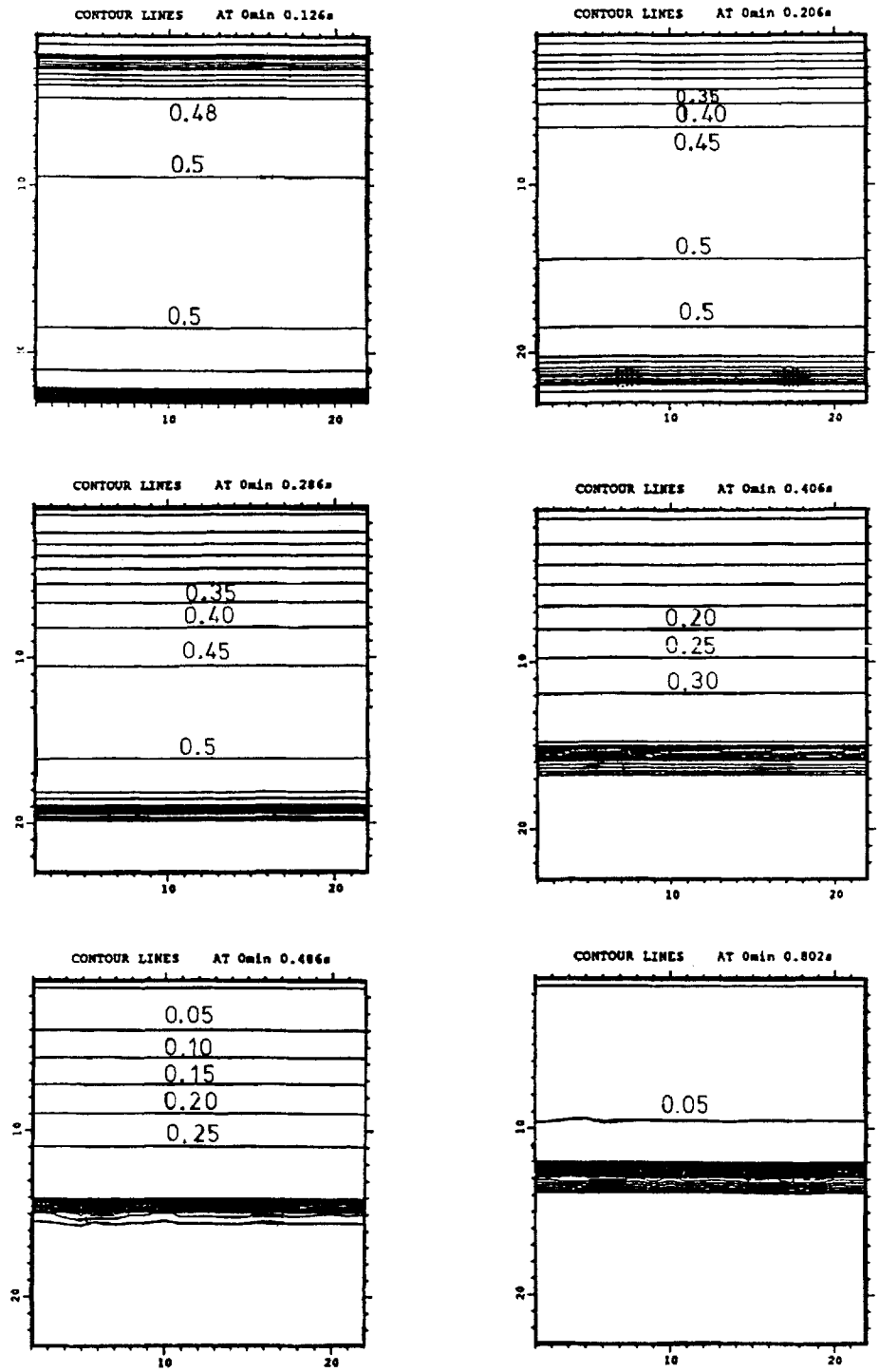

Figure 8. Separation of gas and liquid in a square box

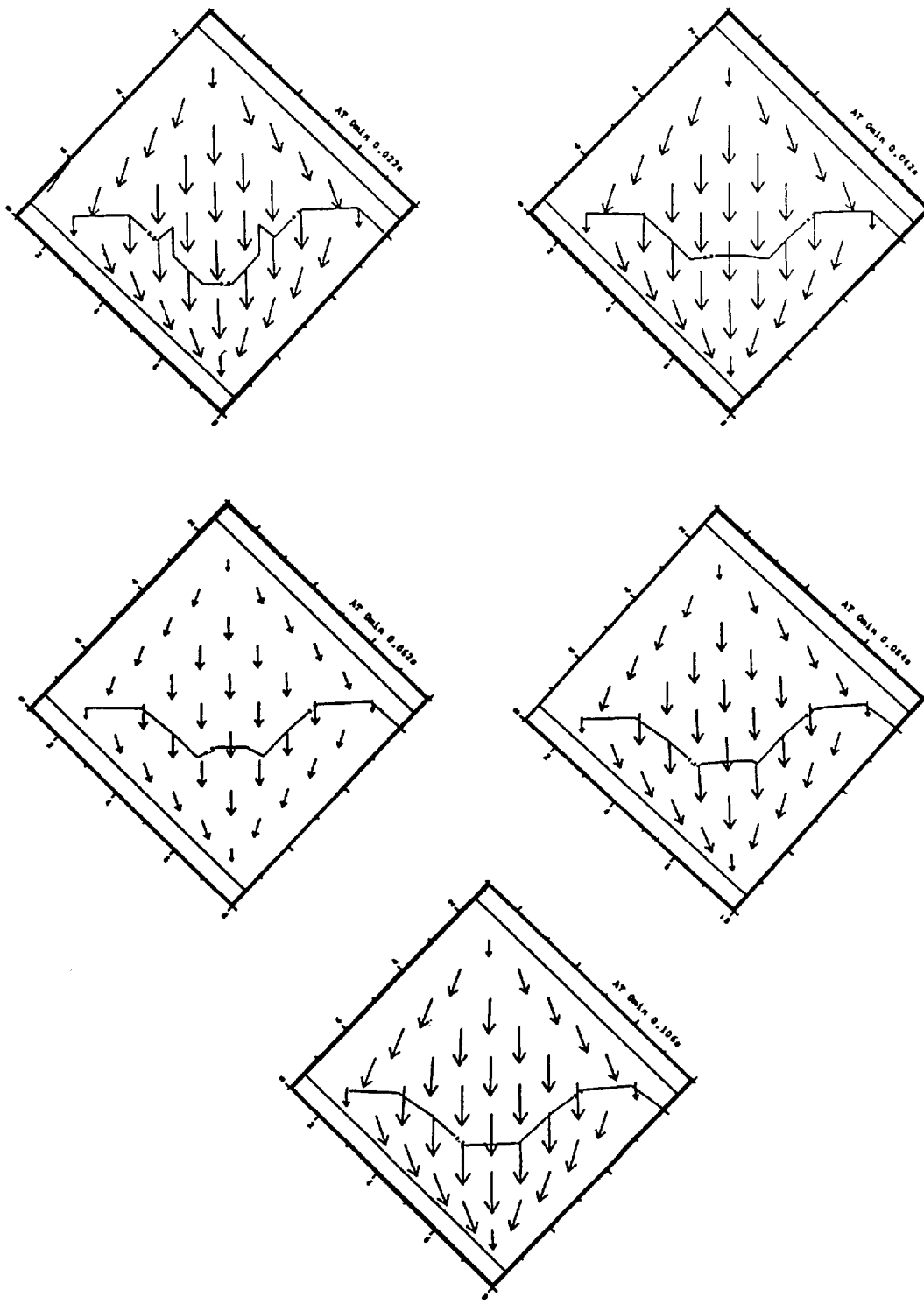

Figure 9. Separation of gas and liquid in a square box tilted 45° to the horizontal

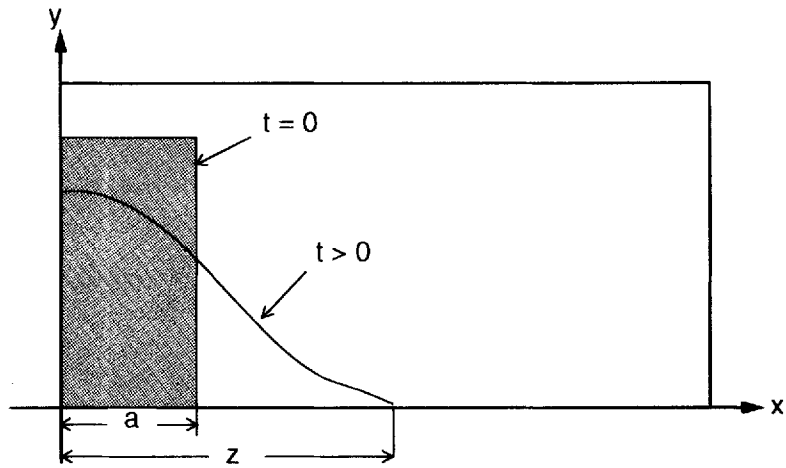

Figure 10. Broken dam problem

Test fluids are water and air with the following properties:

$$\text{density of air} = 1{\cdot}205\ \text{kg m}^{-3}, \qquad \text{density of water} = 998{\cdot}0\ \text{kg m}^{-3},$$

$$\text{viscosity of air} = 1{\cdot}81 \times 10^{-5}\ \text{N s m}^{-2}, \qquad \text{viscosity of water} = 1{\cdot}01 \times 10^{-3}\ \text{N s m}^{-2},$$

at atmospheric conditions.

The applied grid in the simulation consists of 22×40 nodes, uniformly spaced in the x-direction and non-uniformly spaced in the y-direction. The smallest Δy (0·05 m) values are located at the bottom, where the highest resolution is needed to treat the leading edge properly. A time step of 0·002 s has been employed for the computation. Interfacial friction factors from equation (16) were used for this case. The interface is assumed to be located where the volume fraction is 0·5, as suggested by Liu and Spalding.[27]

Due to numerical diffusion, the time evolution of the liquid surface proved to be very sensitive to the numerical dicretization of convective terms in the momentum equations. Consequently, a sensitivity study was performed. Applying the normal interfacial friction factors (16) gives a large diffusion of the leading edge, as indicated by Model 1, Figure 11. Simply omitting the convective term

$$\frac{\partial}{\partial x}(m_k u_k u_k)$$

in equation (61) in cells containing interfaces, only, provides another extreme, limiting numerical diffusion, but obviously yielding erroneous results. The numerical diffusion is due to the discretization, yielding unphysically large convective terms near the leading edge. A practical model was derived by simply reducing the effect of the convective term for low liquid fractions, multiplying it by the volume fraction in the actual cell. The computational results then showed good agreement with the experimental results.

Hirt and Nichols[25] and Liu and Spalding[27] have used another approach to simulate this case. These methods are both basically single-phase calculations, with a discontinuity in the fluid properties representing the interface. The discontinuity or interface position is followed by a 'conserved scalar' which, in principle, is zero or one in either domain of fluid. These methods

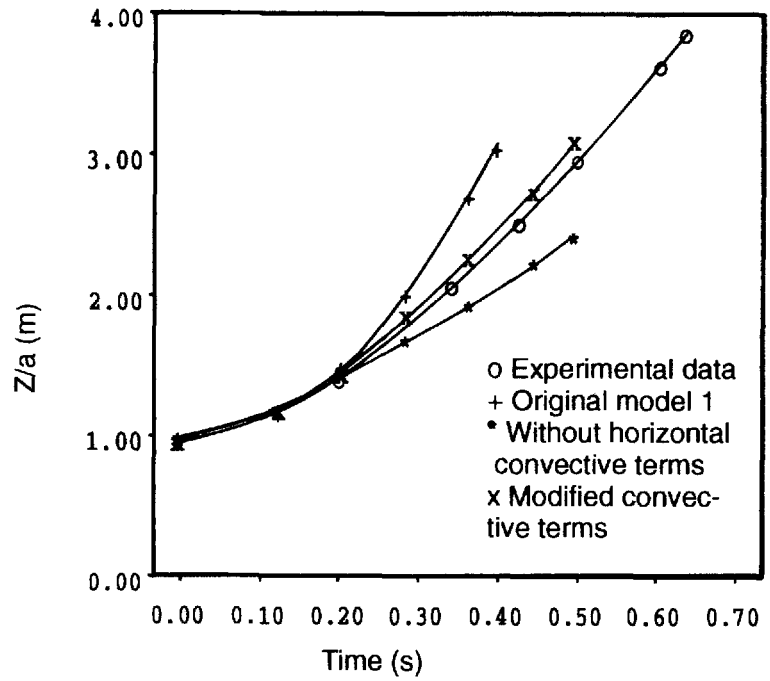

Figure 11. Comparison of the computed Z with the experimental data of Martin and Moyce[28]

avoid numerical diffusion, and reproduce experimental results accurately, but the velocities in each computational mesh have to be equal for both phases.

Collapse of a liquid column. A two-dimensional cavity of side 0·2 m is initially partly filled with liquid and gas. Half the volume is occupied by the liquid on the left side of the cavity, and the interface is aligned with the vertical. Gravity acts in the negative y-direction. The liquid will move from one side to the other over a number of cycles before it comes to rest at the bottom of the cavity.

A uniformly spaced 20×20 grid has been employed with a constant time step of 10^{-3} s. The densities of liquid and gas were set equal to 1000 and 1 kg m^{-3}, respectively, and the viscosity of liquid was 1×10^{-3} Pa s.

The interfacial friction factor applied is given by equation (17), since in this case the movement of the liquid is of equal importance in both directions.

Predictions by the proposed model are compared with those of the FLUENT model[24] in Figure 12. In both calculations the interface is taken to be located where the volume fraction is 0·5. The FLUENT model also applies a full set of two-fluid equations; the solution procedure, however, is quite different as this model applies an iterative solution algorithm based on the SIMPLE method.[4]

The results presented in Figure 12 show very similar time development for the two models.

5. CONCLUSIONS

A numerical two-fluid model has been presented, focusing on a new direct implicit solution method. The numerical solution procedure is based on a first-order semi-implicit finite difference

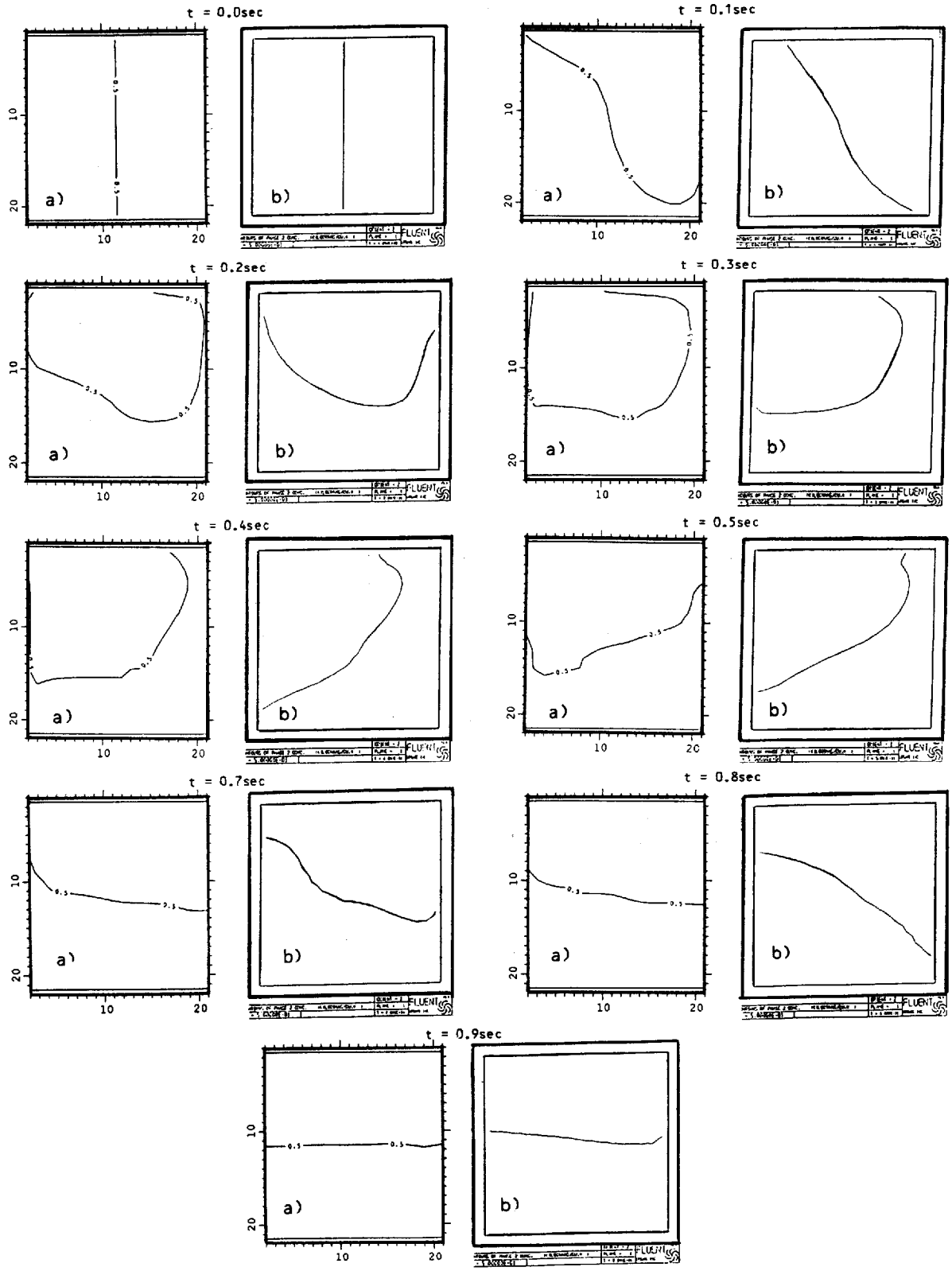

Figure 12. Collapse of a liquid column. Predictions: (a) present model; (b) Boysan[24]

scheme. A staggered mesh or Arakawa C-grid has been applied. The applied method results in a split solution procedure at each time step, where phase velocities and pressures are obtained first, and then specific masses based on densities are updated with new pressures. The proposed scheme is robust, as well as mass, and with a proper correction, also volume conserving.

Comprehensive tests on simple flow problems have been performed to ensure correct implementation of the model and to assess the performance of the numerical scheme.

The single-phase simulations show excellent agreement with analytical solutions for laminar pipe and channel flow.

The model is designed to cover a wide range of stratified flow problems. Four different types of transient two-phase phenomena were simulated. The broken dam and collapsing liquid column problems both provide good tests of the numerical method applied. Model predictions compare very well with the experimental data, and where available, with other methods (FLUENT).

The broken dam problem illustrates the importance of the horizontal convective term in the momentum equation on numerical diffusion.

More comprehensive studies of two-phase stratified and slug flow problems will be presented in a companion paper.

ACKNOWLEDGEMENT

The authors gratefully acknowledge the financial support from the PROFF program, under the Royal Norwegian Council for Scientific and Industrial Research (NTNF). Sponsoring participants were: Total, Shell International Petroleum, Esso Norge a/s, Amoco Norway Oil Company, Elf Acquitane Norge a/s, Saga Petroleum a/s, Statoil, and Norsk Hydro a/s.

APPENDIX I: THE PROPOSED 2D TWO-FLUID MODEL

Volume-averaged equations, expressed in 2D Cartesian co-ordinates (Figure 13), are used for channel flow. Axisymmetric co-ordinates are used to simulate flow in a pipe, with the x-axis along the pipe and the r-axis (y) in the radial direction, as indicated in Figure 14.

Conservation of mass and momentum is then expressed in both frames of reference, as follows:

conservation of mass

$$\frac{\partial}{\partial t}(m_k)+\frac{\partial}{\partial x}(m_k u_k)+\frac{1}{r}\left[\frac{\partial}{\partial y}(r m_k v_k)\right]=0, \tag{60}$$

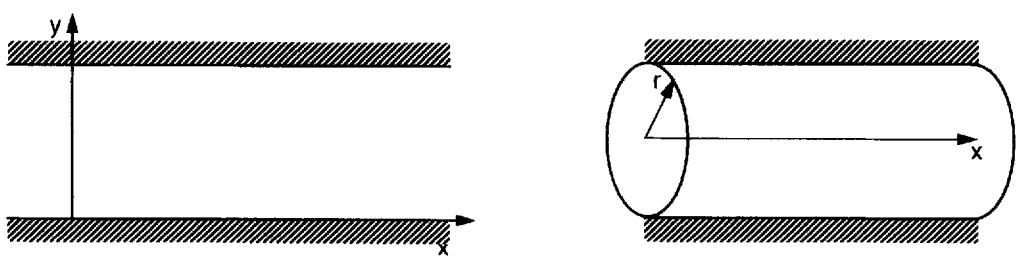

Figure 13. Co-ordinate systems applied in the 2D model (left: Cartesian; right: axisymmetric)

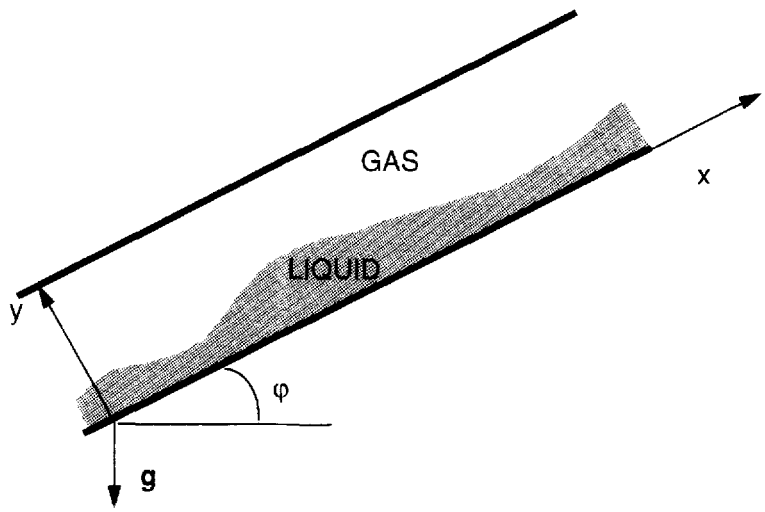

Figure 14. The co-ordinate orientation for channel flow

conservation of momentum for phase k in the x-direction

$$\frac{\partial}{\partial t}(m_k u_k)+\frac{\partial}{\partial x}(m_k u_k u_k)+\frac{1}{r}\frac{\partial}{\partial y}(r m_k u_k v_k)=-\alpha_k\frac{\partial p}{\partial x}-m_k g\cos\varphi+F^x_{ki}|u_r|u_r$$
$$+\frac{\partial}{\partial x}\left(2\alpha_k\mu_{k,\mathrm{eff}}\frac{\partial u_k}{\partial x}\right)+\frac{1}{r}\frac{\partial}{\partial y}\left[r\alpha_k\mu_{k,\mathrm{eff}}\left(\frac{\partial u_k}{\partial y}+\frac{\partial v_k}{\partial x}\right)\right], \quad (61)$$

conservation of momentum for phase k in the y- (or r-) direction

$$\frac{\partial}{\partial t}(m_k v_k)+\frac{\partial}{\partial x}(m_k v_k u_k)+\frac{1}{r}\frac{\partial}{\partial y}(r m_k v_k v_k)=-\alpha_k\frac{\partial p}{\partial y}-m_k g\sin\varphi+F^y_{ki}|v_r|v_r$$
$$+\frac{\partial}{\partial x}\left[2\alpha_k\mu_{k,\mathrm{eff}}\left(\frac{\partial v_k}{\partial x}+\frac{\partial u_k}{\partial y}\right)\right]+\frac{1}{r}\frac{\partial}{\partial y}\left(r\alpha_k\mu_{k,\mathrm{eff}}\frac{\partial r v_k}{\partial y}\right), \quad (62)$$

where $\mu_{k,\mathrm{eff}}$ is the effective viscosity given by (21).

the pressure equation

$$\left(\frac{\alpha_g}{\rho_g}\frac{\partial\rho_g}{\partial p}+\frac{\alpha_\ell}{\rho_\ell}\frac{\partial\rho_\ell}{\partial p}\right)\frac{\partial p}{\partial t}=-\frac{1}{\rho_g}\frac{\partial}{\partial x}(m_g u_g)-\frac{1}{r}\frac{1}{\rho_g}\frac{\partial}{\partial y}(r m_g v_g)-\frac{1}{\rho_\ell}\frac{\partial}{\partial x}(m_\ell u_\ell)-\frac{1}{r}\frac{1}{\rho_\ell}\frac{\partial}{\partial y}(r m_\ell v_\ell). \quad (63)$$

Using x, y with $r=1$ gives the equations in Cartesian co-ordinates, and using x and $y=r$ gives the equations in axisymmetric co-ordinates.

φ denotes the inclination of the pipe or channel relative to the horizontal. The terms F^x_{ki} and F^y_{ki} describe the interfacial momentum transfer between the two phases, in the x- and y-direction, respectively.

There are nine independent main variables, $u_g, v_g, u_\ell, v_\ell, p, \alpha_g, \alpha_\ell, \rho_g, \rho_\ell$, six conservation equations and a volume relation (29). In addition, there are four unknown terms for the interfacial momentum transfer (drag) and turbulent viscosity, which must be specified through closure relations, as described in Section 2.2 and chapter 3.

APPENDIX II: CALCULATION OF VOLUME FRACTIONS AND THE VOLUMETRIC ERROR

The volume fractions are first obtained from the specific mass relations:

$$\alpha_{g,j,i}^{(n+1)'} = \frac{m_{g,j,i}^{n+1}}{\rho_{g,j,i}^{n+1}}, \qquad \alpha_{\ell,j,i}^{(n+1)'} = \frac{m_{\ell,j,i}^{n+1}}{\rho_{\ell,j,i}^{n+1}}. \tag{64}$$

The volume fractions are then redefined to satisfy the volume relation, $\alpha_g = \alpha_\ell = 1$:

$$\alpha_{g,j,i}^{n+1} = \frac{\alpha_{g,j,i}^{(n+1)'}}{\alpha_{g,j,i}^{(n+1)'} + \alpha_{\ell,j,i}^{(n+1)'}}, \qquad \alpha_{\ell,j,i}^{n+1} = 1 - \alpha_{g,j,i}^{n+1}. \tag{65}$$

A volumetric error

$$\Delta_{vol} = 1 - (\alpha_{g,j,i}^{(n+1)'} + \alpha_{\ell,j,i}^{(n+1)'}) \tag{66}$$

may then result, due to discrepancies in the discretization of the volume equation in the first step of the solution, where both masses and directional indices from the previous time step are used, and to the discretization of the mass equations in the second step. By comparing equations (43)–(45), the volumetric error can be expressed as follows:

$$\begin{aligned}
\Delta_{vol} = &-\left[\frac{\alpha_{g,j,i}^{n+1} - \alpha_{g,j,i}^{n}}{\rho_{g,j,i}^{n}}\left(\frac{\partial \rho_g}{\partial p}\right)_{j,i}^{n} + \frac{\alpha_{\ell,j,i}^{n+1} - \alpha_{\ell,j,i}^{n}}{\rho_{\ell,j,i}^{n}}\left(\frac{\partial \rho_\ell}{\partial p}\right)_{j,i}^{n}\right](p_{j,i}^{n+1} - p_{j,i}^{n}) \\
&- \frac{\Delta t}{\Delta x_j}\frac{1}{\rho_{g,j,i}^{n}}\{[(m_g^{n+1}u_g^{n+1})_{j+1,i}^{up} - (m_g^{n}u_g^{n+1})_{j+1,i}^{up}] - [(m_g^{n+1}u_g^{n+1})_{j,i}^{up} - (m_g^{n}u_g^{n+1})_{j,i}^{up}]\} \\
&- \frac{\Delta t}{\Delta x_j}\frac{1}{\rho_{\ell,j,i}^{n}}\{[(m_\ell^{n+1}u_\ell^{n+1})_{j+1,i}^{up} - (m_\ell^{n}u_\ell^{n+1})_{j+1,i}^{up}] - [(m_\ell^{n+1}u_\ell^{n+1})_{j,i}^{up} - (m_\ell^{n}u_\ell^{n+1})_{j,i}^{up}]\} \\
&- \frac{\Delta t}{\Delta y_i}\frac{1}{\rho_{g,j,i}^{n}}\{[(m_g^{n+1}v_g^{n+1})_{j,i+1}^{up} - (m_g^{n}v_g^{n+1})_{j,i+1}^{up}] - [(m_g^{n+1}v_g^{n+1})_{j,i}^{up} - (m_g^{n}v_g^{n+1})_{j,i}^{up}]\} \\
&- \frac{\Delta t}{\Delta y_i}\frac{1}{\rho_{\ell,j,i}^{n}}\{[(m_\ell^{n+1}v_\ell^{n+1})_{j,i+1}^{up} - (m_\ell^{n}v_\ell^{n+1})_{j,i+1}^{up}] - [(m_\ell^{n+1}v_\ell^{n+1})_{j,i}^{up} - (m_\ell^{n}v_\ell^{n+1})_{j,i}^{up}]\}.
\end{aligned} \tag{67}$$

The volumetric error puts additional restrictions on the numerical accuracy and stability. The first term limits the local pressure changes in a given time step, depending upon the compressibility and density of the fluids. Limiting the volumetric error to 10^{-5} and assuming water as the dominating fluid, the model accepts a local pressure transients of 0·1 bar per time step.

The next terms pose no further limitations on the maximum time step in the calculations. This can be seen as follows: Assuming slowly varying velocities in space, observing that $m_k/\rho_k \leqslant 1$, the

remaining parts of (67) reduce to the Courant criterion:

$$\Delta t < \min\left(\frac{\Delta x_j}{u}, \frac{\Delta y_i}{v}\right), \tag{68}$$

where u and v are characteristic phase velocities in the x- and y-direction, respectively. As known, this criterion always applies for the implicit numerical scheme.

APPENDIX III. NOMENCLATURE

A	area
E	energy source
e	internal energy
f	function
$\mathbf{g}$	gravity (body force)
h_l	liquid holdup
H	channel height
l_m	mixing length
$\mathbf{M}$	momentum source
$\mathbf{M}_m^R$	force due to change in mean curvature
$\mathbf{m}_k$	specific mass, phase $k(m_k \equiv \alpha_k \rho_k)$
p	pressure
q	heat flux
r	radial co-ordinate
$\mathbf{R}_{g\ell}$	mean curvature
Re	Reynolds number
$\mathbf{u}$	velocity
u	velocity, x-component
v	velocity, y-component
w	velocity, z-component
x, y, z	Cartesian co-ordinates
α	volume fraction
Γ	mass transfer rate
φ	inclination
λ	bulk viscosity, friction factor
μ	viscosity
ρ	density
σ	surface tension
τ	stress tensor
$\mathfrak{I}$	unity tensor
$\wp$	total stress tensor

Subscripts

g	gas phase
i	interface
i, j	directional indices
k	phase
m	mixture
ℓ	liquid phase

Superscripts

n	time index
R	radius of curvature
T	turbulent
$'$	fluctuating component
$*$	transposed (tensor)

REFERENCES

1. K. Bendiksen, D. Malnes, T. Straume and P. Hedne, 'A non-diffusive numerical model for transient simulation of oil-gas transportation systems', *Proc. 1990 European Simulation Multiconference*, 1990, pp. 508–515.
2. M. T. Philbin, 'The simulation of transient phenomena in multiphase production systems', *IBC Multiphase Operations Offshore Conference*, 1991.
3. G. Ferschneider, M. Lagiere, T. Bourgeois and M. Fitreman, 'How to calculate two-phase flow of gas and oil in pipe lines', Pipe Line Industry, 1985.
4. S. V. Patankar and D. B. Spalding, 'A calculation procedure for heat, mass and momentum transfer in three-dimensional parabolic flows', *Int. J. Heat Mass Transfer*, **15,** 1787–1806 (1972).
5. B. D. Nichols, C. W. Hirt and R. S. Hotchkiss, 'SOLA-VOF: A solution algorithm for transient fluid flow with multiple free boundaries', LA-8355, Los Alamos, 1981.
6. O. Shoham and Y. Taitel, 'Stratified turbulent–turbulent gas–liquid flow in horizontal and inclined pipes', *AIChE J.*, **3,** 377–385 (1984).
7. R. I. Issa, 'Prediction of turbulent, stratified two-phase flow in inclined pipes and channels', *Int. J. Multiphase Flow*, **14,** 141–154 (1988).
8. M. Akai, A. Inoue and S. Aoki, 'The prediction of stratified two-phase flow with a two-equation model of turbulence', *Int. J. Multiphase Flow* **7**, 21–39 (1981).
9. A. Line, L. Masbernat and C. Suzanne, 'Modelling of co-current and counter-current flow of gas and liquid', *Proc. 3rd Int. Conf. on Multi-Phase Flow*, Netherlands, 1987.
10. F. H. Harlow and A. A. Amsden, 'Flow of interpenetrating material phases', *J. Comput. Phys.*, **18,** 440–464 (1975).
11. D. B. Spalding, 'The calculation of free-convection phenomena in gas liquid mixtures,' *Imperial College Mech. Eng. Dept. Report No. HTS/76/11*, 1976.
12. M. B. Carver, 'Numerical computation of phase separation in two fluid flow', *J. Fluids Eng.*, **106,** 1984.
13. R. I. ISSA and A. D. Gosman 'The computation of three-dimensional turbulent two-phase flows in mixture vessels', *Proc. 2nd Int. Conf. Num. Meth. Lam. Turb. Flow*, Pineridge Press, Swansea, 1981.
14. M. K. Looney, R. I. Issa, A. D. Gosman and S. Politis, 'Modelling of the turbulent flow of solid/liquid suspensions in stirred vessels', *Proc. 5th Int. Conf. on Mathematical Modelling*, Berkeley, 1985.
15. K. Bendiksen, D. Malnes, R. Moe and S. Nuland, *The Dynamic Two-Fluid Model OLGA: Theory and Application*, SPE Production Engineers, 1991.
16. N. Zuber and J. A. Findley, 'Averaging volumetric concentration in two-phase flow systems', *J. Heat Transfer*, **87,** 453–468 (1965).
17. G. B. Wallis, *One-dimensional Two-Phase Flow*, McGraw-Hill, New York, 1969.
18. M. Ishii, *Thermo-Fluid Dynamic Theory of Two-Phase Flow*, Eyrolles. 1975.
19. P. H. Vernier and J. M. Delhaye, 'General two-phase flow equations applied to the thermodynamics of boiling water nuclear reactors', *Energie Primaire*, **4,** (1968).
20. D. A. Drew, and R. T. Lahey, 'Application of general constitutive principles to the derivation of multidimensional two-phase flow equations', *Int. J. Multiphase Flow*, **5,** 243–264 (1979).
21. S. Banerjee and A. M. C. Chan, 'Separated flow models– I, analysis of the averaged and local instantaneous formulations', *Int. J. Multiphase Flow*, **6,** 1–24 (1980).
22. S. T. Johansen, 'On the modelling of disperse two-phase flow', *Ph.D. Thesis*, The Norwegian Institute of Technology (NTH), Trondheim, 1990.
23. I. R. Ellull, 'The prediction of dispersed gas–liquid flow in complex pipe geometries', *Ph.D. Thesis*, Imperial College, London, 1989.
24. F Boysan, 'A two-fluid model for FLUENT', Flow Simulation Consultants Ltd., Hutton's Buildings, 146 West Street, Shefield S1 4ES, 1990.
25. C. W. Hirt and B. D. Nichols, 'Volume of fluid (VOF) method for the dynamics of free boundaries', *J. Comput. Phys.*, **39,** 201 (1981).
26. B. E. Launder and D. B. Spalding, *Mathematical Models of Turbulence*, Academic Press, London, 1972.
27. Liu Jun and D. B. Spalding, 'Numerical simulation of flows with moving interfaces', *PCH Phys. Chem. Hydr.*, **10,** 625–637 (1988).

28. J. C. Martin and W. J. Moyce, 'An experimental study of the collapse of liquid column on a rigid horizontal plane', *Phil. Trans. Roy. Soc.*, **244,** 312 (1952).
29. J. Nossen, 'Testing of conjugate gradient-like equation solvers in two-dimensional two-phase flow computation', *IFE/KR/F-91/027*, 1991.
30. G. B. Wallis, 'Annular two-phase flow, Part1', A simple theory, *J. Basic Engineering*, p. 59, 1970.
31. I. Brandt and P. Fuchs, 'Liquid holdup in slugs: some experimental results from the SINTEF two-phase flow laboratory', *Proc. BHRA Conf.*, Nice, France, 1989.